Biophysical Journal
Article

Biophysical Society

Single-Channel Resolution of the Interaction between C-Terminal $Ca_V1.3$ Isoforms and Calmodulin

Elza Kuzmenkina,[1,*] Elena Novikova,[1] Wanchana Jangsangthong,[1] Jan Matthes,[1] and Stefan Herzig[1,2]
[1]Center of Pharmacology, University of Cologne, Cologne, Germany and [2]Cologne University of Applied Sciences, Cologne, Germany

ABSTRACT Voltage-dependent calcium (Ca_V) 1.3 channels are involved in the control of cellular excitability and pacemaking in neuronal, cardiac, and sensory cells. Various proteins interact with the alternatively spliced channel C-terminus regulating gating of $Ca_V1.3$ channels. Binding of a regulatory calcium-binding protein calmodulin (CaM) to the proximal C-terminus leads to the boosting of channel activity and promotes calcium-dependent inactivation (CDI). The C-terminal modulator domain (CTM) of $Ca_V1.3$ channels can interfere with the CaM binding, thereby inhibiting channel activity and CDI. Here, we compared single-channel gating behavior of two natural $Ca_V1.3$ splice isoforms: the long $Ca_V1.3_{42}$ with the full-length CTM and the short $Ca_V1.3_{42A}$ with the C-terminus truncated before the CTM. We found that CaM regulation of $Ca_V1.3$ channels is dynamic on a minute timescale. We observed that at equilibrium, single $Ca_V1.3_{42}$ channels occasionally switched from low to high open probability, which perhaps reflects occasional binding of CaM despite the presence of CTM. Similarly, when the amount of the available CaM in the cell was reduced, the short $Ca_V1.3_{42A}$ isoform showed patterns of the low channel activity. CDI also underwent periodic changes with corresponding kinetics in both isoforms. Our results suggest that the competition between CTM and CaM is influenced by calcium, allowing further fine-tuning of $Ca_V1.3$ channel activity for particular cellular needs.

INTRODUCTION

Voltage-dependent calcium (Ca_V) channels conduct calcium ions into excitable cells upon membrane depolarization. From the family of closely related L-type Ca_V channels ($Ca_V1.1$–$Ca_V1.4$), $Ca_V1.3$ channels activate at most negative voltages, making them suitable to operate at threshold potentials (1). $Ca_V1.3$ channels are expressed in central neurons, endocrine cells, atria and the sinoatrial node of the heart, and cochlear hair cells, in which they regulate spontaneous firing, hormone secretion, pacemaking, and sensory function (2,3).

Loss of $Ca_V1.3$ function in humans and animal models leads to cardiac rhythm disturbances (4–7) and congenital deafness (4,7). Moreover, $Ca_V1.3$ knockout mice show deficiencies in some functions of the amygdala and hippocampus (8–10).

Gain of $Ca_V1.3$ function is associated with pathological conditions, such as Parkinson's (11,12) and Alzheimer's diseases (13), prostate and other cancers (14), some cases of aldosteronism (15,16), autism spectrum disorders, and epilepsy (17–20).

The function of $Ca_V1.3$ channels is tightly regulated by protein interactions with its C-terminus (21–23). Fig. 1 schematically depicts $Ca_V1.3$ channels and their C-terminal domains. A proximal part of the C-terminus comprises segments critical for calcium-dependent inactivation (CDI) of the channels: EF-hand and PreIQ-IQ domains. The current view is that, in CDI, local intracellular calcium concentration is sensed by a small protein calmodulin (CaM) attached to PreIQ-IQ domains of the channel (24). CaM consists of two lobes, each containing two EF-hands with high affinity for Ca^{2+} (25). Binding of calcium to CaM reduces channel open probability (26) caused by the reallocation of CaM on the proximal C-terminus with reattachment of one of its lobes to the low-affinity CaM-binding site in the N-terminus, NSCaTE (27). The EF-hand motif upstream from the CaM-binding sites in the channel C-terminus was proposed to be required for a transmission of CaM motions into CDI (28).

Here, we focus on the interaction between the distal C-terminus and CaM regulation of the channel. The distal C-terminus of $Ca_V1.3$ channels contains a C-terminal

Submitted September 17, 2018, and accepted for publication January 16, 2019.

*Correspondence: elza.kuzmenkina@uk-koeln.de
Elza Kuzmenkina and Elena Novikova contributed equally to this work.

Editor: Henry M. Colecraft.
https://doi.org/10.1016/j.bpj.2019.01.025

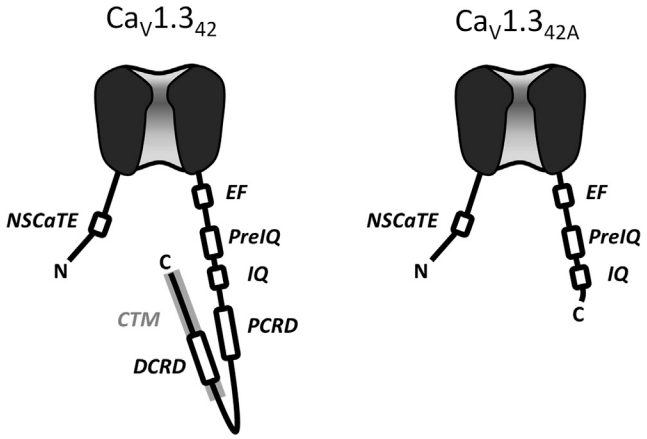

FIGURE 1 Schematic representation of $Ca_V1.3$ N- and C-terminal domains involved in CDI and gating regulation by CaM. Two $Ca_V1.3$ naturally occurring splice variants ($Ca_V1.3_{42}$ and $Ca_V1.3_{42A}$) differ in the length of the C-terminus.

modulator domain (CTM). In L-type Ca^{2+} channels, CTM reduces current density and shifts the activation to more positive potentials (29–33). Furthermore, CTM hinders voltage-dependent facilitation of $Ca_V1.3$ channels (34,35). Finally, in $Ca_V1.3$ and $Ca_V1.4$ channels, CTM inhibits CDI (32,33,36–39). As the underlying mechanism, it was proposed that intramolecular binding of CTM to the proximal C-terminus competitively hinders the binding of CaM (32,33,40). In particular, charge interactions between the conserved distal C-terminal regulatory domain (DCRD) in the CTM and the proximal C-terminal regulatory domain (PCRD) in the proximal C-terminus downstream from the IQ domain are important (32,33).

Several splice variants of $Ca_V1.3$ C-terminus are expressed simultaneously in brain, heart, and other tissues (33,37,38). At least eight isoforms were found in the complementary DNA library of the rat brain, which were different regarding the presence of IQ domain, PCRD, and DCRD (38). Such a diversity of $Ca_V1.3$ channels may be involved in the fine-tuning of calcium influx and signaling for cell requirements (41–43).

In this work, we utilized single-channel resolution to better understand the mechanism by which $Ca_V1.3$ CTM variants differ in their gating (27,37). We compared the two most distinct splice variants after the expression in HEK-293 cells: the long $Ca_V1.3_{42}$ with the full-length C-terminus and the short $Ca_V1.3_{42A}$ with the C-terminus truncated shortly after the IQ domain (Fig. 1).

MATERIALS AND METHODS

Plasmids

Vectors containing human $Ca_V1.3_{42}$, $Ca_V1.3_{42A}$, rat $Ca_V\beta_3$, and rabbit $Ca_V\alpha_2\delta$-1 were described previously (33,37). pcDNA3 plasmid with the wild-type rat CaM was described in Peterson et al. (25). $BSCaM_{IQ}$, a fluorescent reporter derived from neuromodulin, which binds CaM with high affinity via its IQ motif, was expressed in pcDNA3.1 vector (40,44).

Cell culture and transfection

HEK-293 cells were cultured as described previously (37). For single-channel measurements, $Ca_V1.3$ channels were transiently expressed in HEK-293 cells. Complementary DNA was delivered into the cells using Effectene transfection (QIAGEN, Hilden, Germany) or calcium phosphate precipitation (45). Plasmid mixtures contained the following: 1) 2 μg $Ca_V1.3_{42}$ or $Ca_V1.3_{42A}$ α1, 1 μg $Ca_V\beta_3$, 1.5 μg $Ca_V\alpha_2\delta$-1, and 0.5 μg green fluorescent protein (GFP) (Effectene transfection); 2) 1 μg $Ca_V1.3_{42}$ or $Ca_V1.3_{42A}$ α1, 0.5 μg $Ca_V\beta_3$, 0.75 μg $Ca_V\alpha_2\delta$-1, 1 μg CaM, and 0.5 μg GFP (calcium phosphate precipitation); or 3) 1 μg $Ca_V1.3_{42}$ or $Ca_V1.3_{42A}$ α1, 0.5 μg $Ca_V\beta_3$, 0.75 μg $Ca_V\alpha_2\delta$-1, 1 μg $BSCaM_{IQ}$, and 0.5 μg GFP (calcium phosphate precipitation). GFP plasmid was added to visualize the transfections (37).

Single-channel patch-clamp recordings

$Ca_V1.3$ currents were recorded at room temperature in the cell-attached patch-clamp configuration from GFP-positive cells 48–72 h after transfection as described previously (37). Depolarizing bath solution contained (in mM) 120 potassium glutamate, 25 KCl, 2 $MgCl_2$, 10 HEPES, 2 EGTA, 1 $CaCl_2$, 1 Na_2ATP, and 10 dextrose (pH 7.4 with KOH). For experiments with a calcium agonist, the bath solution additionally contained 1 μM (S−) Bay K 8644. Patch pipettes made from borosilicate glass were coated with Sylgard and typically had a resistance of 7–10 MΩ. The pipette solution contained (in mM) 15 $BaCl_2$ or 15 $CaCl_2$, 105 tetraethanolamine-Cl, and 10 HEPES (pH 7.4 with tetraethanolamine-OH). The clamped patches were hold at −100 mV. Depolarizing test potentials were applied for 150 ms at a frequency of 1.67 Hz. Single-channel currents were filtered at 2 kHz (−3 decibel, four-pole Bessel) and sampled at 10 kHz. For Ba^{2+} measurements, some results from five of seven experiments with $Ca_V1.3_{42}$ and six of seven experiments with $Ca_V1.3_{42A}$ were published previously (37). However, this article presents a more detailed analysis of the data.

For every test potential, data were recorded over a period of at least 108 s (180 sweeps). The number of channels was estimated by the highest level of stacked openings. The recorded experiments contained one channel, except experiments with overexpression of CaM (two of six patches contained two channels as judged by the stacked openings) and $BSCaM_{IQ}$ (1 of 12 patches contained two channels). Single-channel gating analysis was performed as reported previously (46). In the following, t_O denotes open time either from an individual event or the mean value as specified in the context. Similarly, P_O denotes open probability either from an individual sweep or the mean value as specified. Mean active P_O refers to the mean open probability calculated from nonblank (active) sweeps.

For the CDI analysis, each sweep was split in early and late windows (0–50 and 50–150 ms, respectively). CDI_{PO} values were defined as $1–P_{O\ 50–150\ ms}$/maximal ($P_{O\ 0–50\ ms}$, $P_{O\ 50–150\ ms}$), where P_O can be a value from an individual sweep or a mean or smoothed value as specified in point. In particular, to reduce the noise, the Gaussian filtering was applied to P_O diaries before CDI_{PO} calculations. Note, we did not perform any smoothing or averaging of CDI_{PO} values; all operations were performed with P_O values, and then they were used for CDI_{PO} calculations.

Segmentation of open probability and CDI diaries

The per sweep open probability diaries were segmented into clusters with statistically different single-channel activity using a bottom-up merging strategy as described previously (47). The segmentation procedure stopped when the mean channel P_O of neighboring clusters were distinct ($p < 0.05$) by the permutation test. The clusters were classified as belonging to the

low- or high-P_O state, depending on the mean active P_O of a given cluster. The threshold for the separation between the low- or high-P_O states was set manually as described in Fig. 3.

CDI diaries were calculated from CDI_{PO} values, where P_O values were calculated either from individual sweeps or from P_O diaries smoothed by the long-pass Gaussian filter with a cutoff frequency of 0.33 Hz. For the segmentation procedure, however, $P_{O\ 0–50\ ms}$ and $P_{O\ 50–150\ ms}$ diaries were used. The bottom-up merging of the sweeps proceeded until the CDI_{PO} values of the neighboring clusters calculated using mean $P_{O\ 0–50\ ms}$ and $P_{O\ 50–150\ ms}$ were distinct ($p < 0.05$) by the permutation test. The clusters were classified as belonging to the low- or high-CDI state, depending on the CDI_{PO} calculated with mean P_O values of a given cluster. The threshold for the separation between the low- or high-CDI states was set manually as described in Fig. 5.

Calculation of lifetimes

Lifetimes of low- or high-P_O (CDI) states were calculated as the total observation time of the respective type of the channel activity divided by the number of transitions from the given type of the channel activity to a different channel activity (from low to high or from high to low). Corrected observation times and the number of transitions for the two-channel experiments were calculated as described in the Supporting Materials and Methods. SEs of the logarithm of the lifetimes were estimated by the jackknife method (this corresponds to the geometric mean ± SE factors of the mean lifetimes). The logarithms of the lifetimes were statistically compared using an exact permutation test. We did not perform corrections for the missed transitions in our lifetime calculations.

RESULTS

Dynamic competition between CTM and CaM

$Ca_V1.3_{42}$ and $Ca_V1.3_{42A}$ splice variants differ in the length of their C-terminus (Fig. 1). As we have shown previously, the long C-terminus $Ca_V1.3_{42}$ isoform has markedly reduced single-channel open probability as compared with the short C-terminus $Ca_V1.3_{42A}$ isoform (37). In these experiments, single-channel currents (Fig. S1) were evoked by stepping from the holding potential of −100 mV to the various test potentials with 15 mM Ba^{2+} as a charge carrier. However, sweep-by-sweep inspection of the open probability (P_O) diaries revealed that $Ca_V1.3_{42}$ occasionally switched from the low- to the high-open-probability gating, similar to the typical activity of $Ca_V1.3_{42A}$ (Fig. 2, *A* and *B*).

It was previously proposed that high activity of $Ca_V1.3_{42A}$ is because of the binding of CaM with no Ca^{2+} ions bound to it (apoCaM) to the channel's C-terminus, and the low activity of $Ca_V1.3_{42}$ corresponds to its basal activity in the absence of CaM because the intramolecular binding of CTM to the proximal C-terminus hinders the attachment of CaM (27). Our data suggest a dynamic competition between CTM and CaM binding on a minute timescale. To substantiate this hypothesis, we performed experiments with an altered availability of the intracellular CaM. Overexpression of the wild-type CaM with $Ca_V1.3_{42}$ resulted in a slight increase of the single-channel open probability as compared to the experiments with endogenous CaM (37) (Fig. 2, *C* and *E*, exemplary recordings shown in Fig. S1). Consistently, the reduction of the freely available endogenous CaM by the coexpression of the CaM-binding $BSCaM_{IQ}$ (44) led to a decrease of the activity of $Ca_V1.3_{42A}$ and the appearance of switching between periods of high and low open probability (Fig. 2, *D* and *F*, exemplary recordings shown in Fig. S1).

To quantify the rates of the transitions between high-P_O (bound-CaM-like) and low-P_O (no-CaM-like) states, we needed quantitative boundaries for the definition of high and low channel activity. Therefore, we built histograms of the logarithm of the channel open probability in individual sweeps. For $Ca_V1.3_{42}$ channels, we observed a large peak at low-P_O values and a small peak at high-P_O values (Fig. 3 *A*), confirming the presence of two separate gating states. For $Ca_V1.3_{42A}$ channels, P_O distributions were dominated by a peak at high values (Fig. 3 *B*). For $Ca_V1.3_{42}$ + CaM and $Ca_V1.3_{42A}$ + $BSCaM_{IQ}$ experiments, P_O distributions were broad, covering both high and low values (data not shown). The threshold between high and low channel activity was manually set in the minimum between the low-P_O peak of $Ca_V1.3_{42}$ and the high-P_O peak of $Ca_V1.3_{42A}$. Then, P_O diaries were split in time clusters with statistically distinct channel open probability (Fig. 3, *C* and *D*), in which mean active P_O (i.e., mean P_O of all but blank sweeps) was used to categorize clusters as belonging to the high- or low-P_O states. Time clusters of P_O also confirmed the visual impression that high- and low-P_O states were likely comprised from multiple substates with distinct channel activity. However, because the data did not allow us to separate substates from each other by a threshold approach, the clusters were fused together to yield periods of continuous residence in the high- and low-P_O states.

The survival curves of high- and low-P_O periods decayed monoexponentially (Fig. 3, *E* and *F*), confirming sufficiency of single aggregate high- and low-P_O state definitions in the model and appropriate homogeneity of the data.

Manipulations with the intracellular CaM concentration altered mean lifetimes of the high- and low-P_O states in agreement with the hypothesis of the competition between CTM and CaM. Overexpression of CaM led to the increase and overexpression of $BSCaM_{IQ}$ led to the decrease of the low-P_O (no-CaM-like) state lifetimes, whereas mean lifetimes of the high-P_O (bound-CaM-like) state remained unaffected (Table 1). Furthermore, lifetimes appeared to be voltage independent (data not shown).

CTM effects on CDI

CDI is a negative feedback mechanism to cease a potentially toxic Ca^{2+} influx on a millisecond timescale. Local Ca^{2+} is sensed by a CaM molecule tethered to the C-terminus of the channel. It was proposed that upon the binding of Ca^{2+} ions to CaM, CaM changes its position on the channel C-terminus, inducing different channel gating (48). To study CTM effects on CDI, we performed single-channel experiments

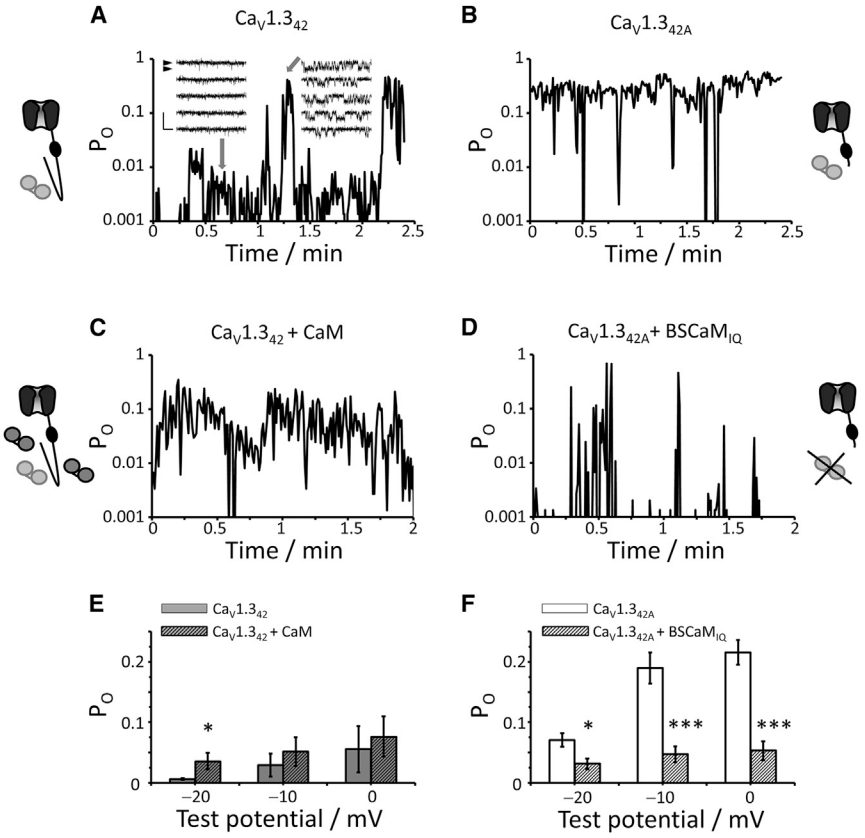

FIGURE 2 At equilibrium, single $Ca_V1.3$ channels experience fluctuation of the channel activity depending on the CaM accessibility. 15 mM Ba^{2+} was used as a charge carrier. Depolarizing voltage steps from a holding potential of −100 mV to test potentials of −20, −10, and 0 mV were applied for 150 ms every 600 ms. (*A–D*) Exemplary single-channel P_O diaries for $Ca_V1.3_{42}$ (*A*), $Ca_V1.3_{42A}$ (*B*), $Ca_V1.3_{42}$ + CaM (*C*), and $Ca_V1.3_{42A}$ + $BSCaM_{IQ}$ (*D*) are shown. Each of the two inserts in (*A*) shows five consecutive sweeps of current recordings at different time points of the same experiment. One sweep corresponds to one point in the P_O diary. The first inset demonstrates low channel activity at 0.6 min, whereas the second inset highlights high activity at 1.3 min (Scale bars, vertical is 2 pA and horizontal is 20 ms. *Black triangle arrows* indicate closed- and open-state current levels). Shown examples were obtained at 0 mV test potential. (*Pictograms in* (*A*)–(*D*)) Channels with long and short C-termini symbolize $Ca_V1.3_{42}$ and $Ca_V1.3_{42A}$, respectively. The black oval in the channel's proximal C-terminus depicts CaM-binding sites (PreIQ-IQ domains). Light and dark two-lobe proteins represent endogenous and transfected CaM molecules, respectively. Crossed-out CaM molecules depict CaM bound to $BSCaM_{IQ}$. (*E*) Overexpression of CaM with $Ca_V1.3_{42}$ channels resulted in a slight increase of the channel open probability. Gray bars and hatched bars show means ± SE from recordings with $Ca_V1.3_{42}$ (n = 7) and $Ca_V1.3_{42}$ + CaM (n = 6), respectively. $*p < 0.05$ for comparing $Ca_V1.3_{42}$ and $Ca_V1.3_{42}$ + CaM by Student's *t*-test. (*F*) Overexpression of $BSCaM_{IQ}$ with $Ca_V1.3_{42A}$ channels led to a marked suppression of high channel activity. White bars and hatched bars show means ± SE from recordings with $Ca_V1.3_{42A}$ (n = 7) and $Ca_V1.3_{42A}$ + $BSCaM_{IQ}$ (n = 12), respectively. * and $***p < 0.05$ and $p < 0.001$, respectively, for comparing $Ca_V1.3_{42A}$ and $Ca_V1.3_{42A}$ + $BSCaM_{IQ}$ by Student's *t*-test.

with 15 mM Ca^{2+} as a charge carrier. Exemplary recordings are shown in Figs. 4 *A* and S2 *A*. CDI was visible as a decline of the channel activity and, respectively, decay of the average current at the end of the test pulse (Figs. 4 *A* and S2, *A* and *B*). Furthermore, CDI manifested itself as the reduction of the channel open time during the test pulse (Fig. 4 *B*) (26,49).

At 0 mV test voltage, single $Ca_V1.3_{42}$ showed markedly reduced current inactivation compared to $Ca_V1.3_{42A}$ channels, reflecting CDI inhibition by CTM (Fig. 4 *C*). Surprisingly, the difference in CDI between $Ca_V1.3$ isoforms disappeared at more negative potentials (Fig. S2 *B*). However, these data have to be interpreted with caution because of very low current amplitudes. Therefore, we focused on the analysis of CTM effects on CDI at 0 mV. Every sweep was split into two windows: an early window from 0 to 50 ms, containing the current peak, and a late window from 50 to 150 ms, in which the current is inactivated by CDI. For both $Ca_V1.3$ isoforms, mean P_O and open time were lower in the late window as in the early window, but for $Ca_V1.3_{42A}$, the reduction was more pronounced and statistically significant (Fig. 4 *D*). An advantage of the window-statistics analysis of CDI over the peak-to-plateau decay analysis is the use all events for the statistical analysis and that all calculations are additive.

Actually, if CTM was able to almost completely prevent CaM tethering to the channel C-terminus as it occurred with Ba^{2+} as charge carrier, we would expect only small CDI for $Ca_V1.3_{42}$ isoform. To gain more insight into the dynamic of CTM interaction with Ca^{2+} as a charge carrier, we plotted sweep-by-sweep diaries of CDI (Fig. 5, *A* and *B*). As a measure of CDI, we introduced $CDI_{PO} = 1 - P_{O,\ late}/\max(P_{O,\ early}, P_{O,\ late})$. However, generally low open probability with Ca^{2+} as a charge carrier means a low number of events in each sweep and thus high noise of CDI_{PO}. To cope with this problem, we smoothed P_O diaries using a low-pass Gaussian filter and then calculated CDI_{PO} from those filtered data (*blue lines* in Fig. 5, *A* and *B*). The diaries of the smoothed CDI_{PO} revealed that $Ca_V1.3_{42}$ channels were fluctuating between high and low CDI, whereas $Ca_V1.3_{42A}$ channels showed predominantly high CDI (Fig. 5, *A* and *B*). Similarly to the analysis of Ba^{2+} data, we built pooled histograms of smoothed CDI_{PO} to define a threshold between high and low CDI (Fig. 5, *C* and *D*). Remarkably, the fraction of sweeps with high CDI for $Ca_V1.3_{42}$ from Ca^{2+} data (0.59 ± 0.15, n = 5) was larger than the fraction

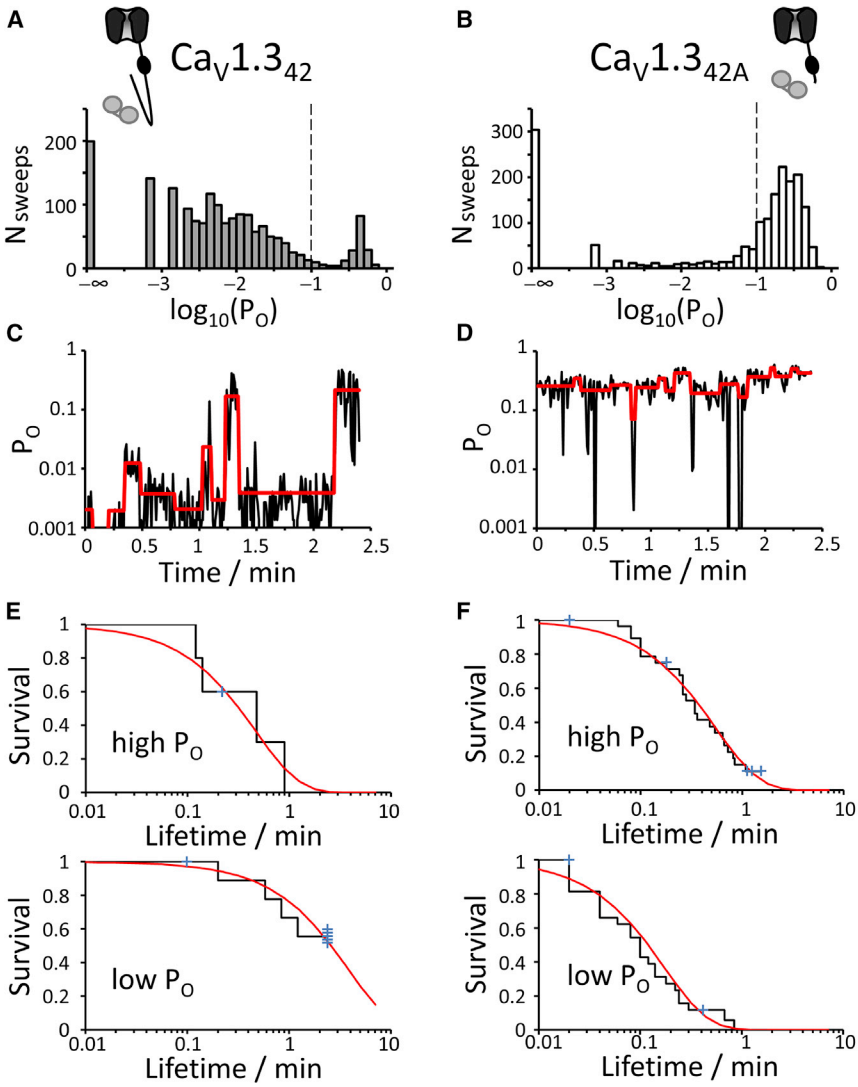

FIGURE 3 Exemplary analysis of the lifetimes of high- and low-P_O states at 0 mV test potential. (*A* and *B*) Pooled histograms of $\log_{10}(P_O)$ were used to define a threshold separating high and low P_O. It was manually set at the minimum between a low-P_O peak of $Ca_V1.3_{42}$ (*A*) and a high-P_O peak of $Ca_V1.3_{42A}$ (*B*). N_{sweeps} denotes the number of sweeps. (*C* and *D*) An agglomerative clustering procedure was applied to P_O diaries to identify periods with distinct channel activity. (*C*) and (*D*) display results of the clustering for the examples shown in Fig. 2 *A* ($Ca_V1.3_{42}$) and Fig. 2 *B* ($Ca_V1.3_{42A}$), respectively. Red stepped lines show the mean active P_O of the resulted clusters. Clusters with the mean active P_O above the threshold belong by our definition to the state of the high P_O, and, vice versa, clusters with mean active P_O below the threshold belongs to the state of the low P_O. (*E* and *F*) Survival curves of the low- and high-P_O states for $Ca_V1.3_{42}$ (*E*) and $Ca_V1.3_{42A}$ (*F*) fit well to a monoexponential function. Black stepped lines are Kaplan-Meier estimations from the pooled data. Blue crosses indicate censored observations. Red smooth lines are exponential curves with decay constants equal to the calculated lifetimes of the high- and low-P_O states (Table 1).

of sweeps with high P_O from Ba^{2+} data (0.11 ± 0.09, $n = 7$, $p = 0.012$). This suggests that the CTM competition with CaM can be attenuated by Ca^{2+} ions.

To assess whether CaM association or dissociation rates were affected, we analyzed lifetimes of high- and low-CDI states. We applied a clustering procedure to split CDI_{PO} diaries into segments with statistically different CDI_{PO} and then categorized them as belonging to high- or low-CDI states using the threshold (*red lines* in Fig. 5, *A* and *B*). We did not detect deviations from the monoexponential behavior in the survival curves of the high- and low-CDI states (Fig. 5, *E* and *F*).

For $Ca_V1.3_{42}$, the lifetime of the high-CDI state (Table 2) was similar to the lifetimes of high-P_O states for $Ca_V1.3_{42}$ and $Ca_V1.3_{42A}$ isoforms when Ba^{2+} as a charge carrier was used (Table 1). For $Ca_V1.3_{42A}$, the lifetime of the

TABLE 1 Lifetimes of the High- and Low-P_O States for $Ca_V1.3$ Channels with 15 mM Ba^{2+} as a Charge Carrier at 0 mV Test Potential

	Lifetime (min)			
	$Ca_V1.3_{42}$	$Ca_V1.3_{42A}$	$Ca_V1.3_{42}$ + CaM	$Ca_V1.3_{42A}$+ $BSCaM_{IQ}$
High-P_O state	0.47×/1.2	0.55×/1.2	0.20×/1.5	0.43×/1.3
Low-P_O state	3.7×/2.3	0.17×/1.4**	1.3×/2.3	1.7×/1.6##

Lifetimes were calculated from the pooled data based on the clustering of the P_O diaries (see Fig. 3, *C* and *D*). Respective geometric mean SE factors are given after "times or divided by" symbols. The numbers of cells were 7, 7, 6, and 12 for $Ca_V1.3_{42}$, $Ca_V1.3_{42A}$, $Ca_V1.3_{42}$ + CaM, and $Ca_V1.3_{42A}$ + $BSCaM_{IQ}$ experiments, respectively. Statistical significance was checked by an exact permutation test applied to the logarithm of the lifetimes. ** denote $p < 0.01$ for comparing $Ca_V1.3_{42A}$ or $Ca_V1.3_{42}$ + CaM with $Ca_V1.3_{42}$. ## denote $p < 0.01$ for comparing $Ca_V1.3_{42A}$ and $Ca_V1.3_{42A}$ + $BSCaM_{IQ}$.

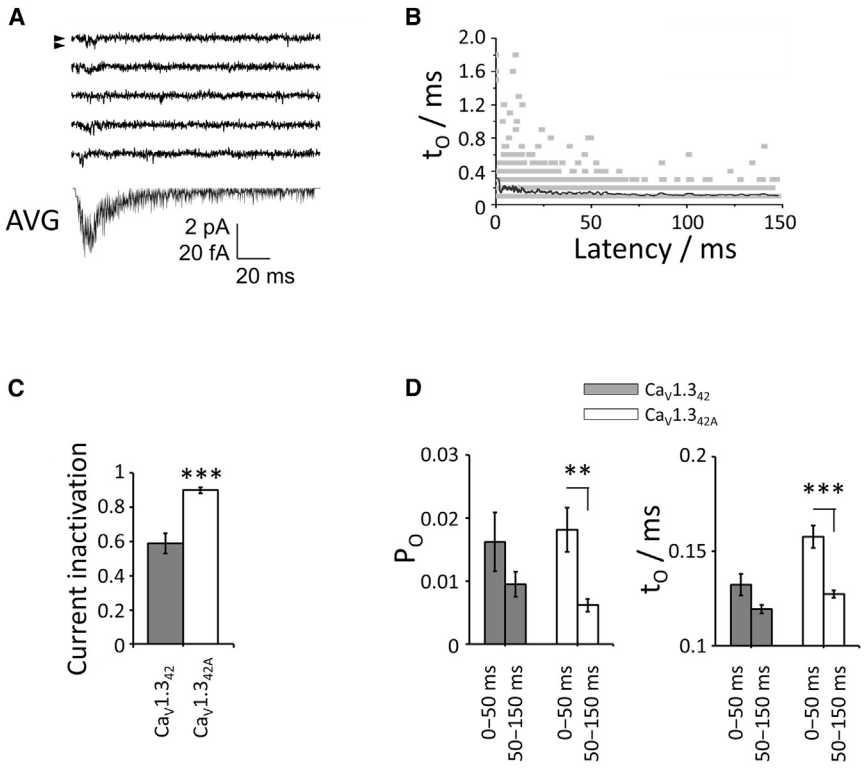

FIGURE 4 CDI of single $Ca_V1.3$ channels at 0 mV test potential. 15 mM Ca^{2+} was used as a charge carrier. The voltage protocol was the same as for Ba^{2+} measurements. (*A*) An example of single $Ca_V1.3_{42A}$ channel currents at 0 mV test voltage is shown. Five consecutive sweeps are shown. Black triangle arrows indicate closed- and open-state current levels. The lowest trace (AVG) is the average current of all 300 consecutive sweeps at 0 mV for this cell. The vertical scale bar is 2 pA for the sweeps and 20 fA for the average current. (*B*) A scatter plot of the event open times versus latency demonstrates the shortening of the open time during the test pulse as a result of CDI. Individual data symbols represent one opening event. The black line is the moving average of 50 events. The data are shown for the same example as in (*A*). (*C*) The inactivation of the average single-channel Ca^{2+} currents at 150 ms for $Ca_V1.3_{42}$ (*gray bars*, n = 5) and $Ca_V1.3_{42A}$ (*white bars*, n = 7) channels at 0 mV is shown. The behavior of the isoforms was significantly different (***$p < 0.001$ by Student's *t*-test). Data are reported as mean ± SE. (*D*) A test potential of 0 mV was used to study CDI of isoforms in more detail. For $Ca_V1.3_{42A}$ channels (*white bars*), the mean P_O was higher, and the mean open time was longer at the beginning (0–50 ms) than at the end (50–150 ms) of the test pulse. For $Ca_V1.3_{42}$ channels (*gray bars*), the difference between the beginning and the end of the test pulse appeared to be smaller and did not reach statistical significance. ** and ***$p < 0.01$ and $p < 0.001$, respectively, for comparing mean values at the beginning (0–50 ms) and end (50–150 ms) of the test pulse by paired Student's *t*-test.

high-CDI state appears to be increased but this may be an artifact due to missed low-CDI events.

By contrast, the lifetime of the low-CDI state of $Ca_V1.3_{42}$ channels was less than the lifetime of the low-P_O state of $Ca_V1.3_{42}$ channels with Ba^{2+} as a charge carrier. For $Ca_V1.3_{42A}$ channels, however, lifetimes of the Ca^{2+} low-CDI and Ba^{2+} low-P_O states were similar (Tables 1 and 2). Thus, our results suggest that, in the presence of calcium ions, CTM becomes less effective in hindering the CaM association. In agreement with this hypothesis, the application of the calcium agonist (S−) Bay K 8644 further minimized the difference between the single-channel calcium currents of the $Ca_V1.3$ isoforms (Fig. S3).

CDI mechanism

Until recently, CDI was explained as relocation of CaM upon calcium binding from its silent preassociation site to Ca^{2+}/CaM effector sites, leading to a channel state with reduced openings (48). However, in the view of new findings that apoCaM association is not a silent process but results in the strongly increased channel activity (27), a novel hypothesis of CDI mechanism has emerged: Upon binding of calcium ions, CaM changes its conformation or attachment position and the channel returns to its original low activity; when calcium concentration drops and the attached CaM loses calcium ions, the channel becomes strongly active again (27). We investigated whether our data are consistent with this hypothesis. Therefore, we compared the level of the channel activity from the sweeps with low CDI and the level of the channel activity of the sweeps with high CDI. Indeed, the open probability of high-CDI sweeps at the beginning of the test pulse was higher than the open probability of low-CDI sweeps (Fig. 6). This is in line with the assumption that the main effect of apoCaM association is the boosting of the channel activity not only for Ba^{2+} but also for Ca^{2+} as a charge carrier. At the end of the test pulse, the open probability of the high-CDI sweeps fell to approximately the same level as in the channels with the low CDI (Fig. 6). The reduction of the open time as a result of CDI can be explained similarly. Open time in high-CDI sweeps at the end of the test pulse dropped to the open-time values of low-CDI (no-CaM) sweeps (Fig. 6). Thus, our data are consistent with the postulated mechanism of CDI.

DISCUSSION

Dynamic competition between CaM and CTM

Alternative splicing of the C-terminus of $Ca_V1.3$ channels results in channels with strikingly different gating properties (33,37,38). Yue and co-workers revealed that both the

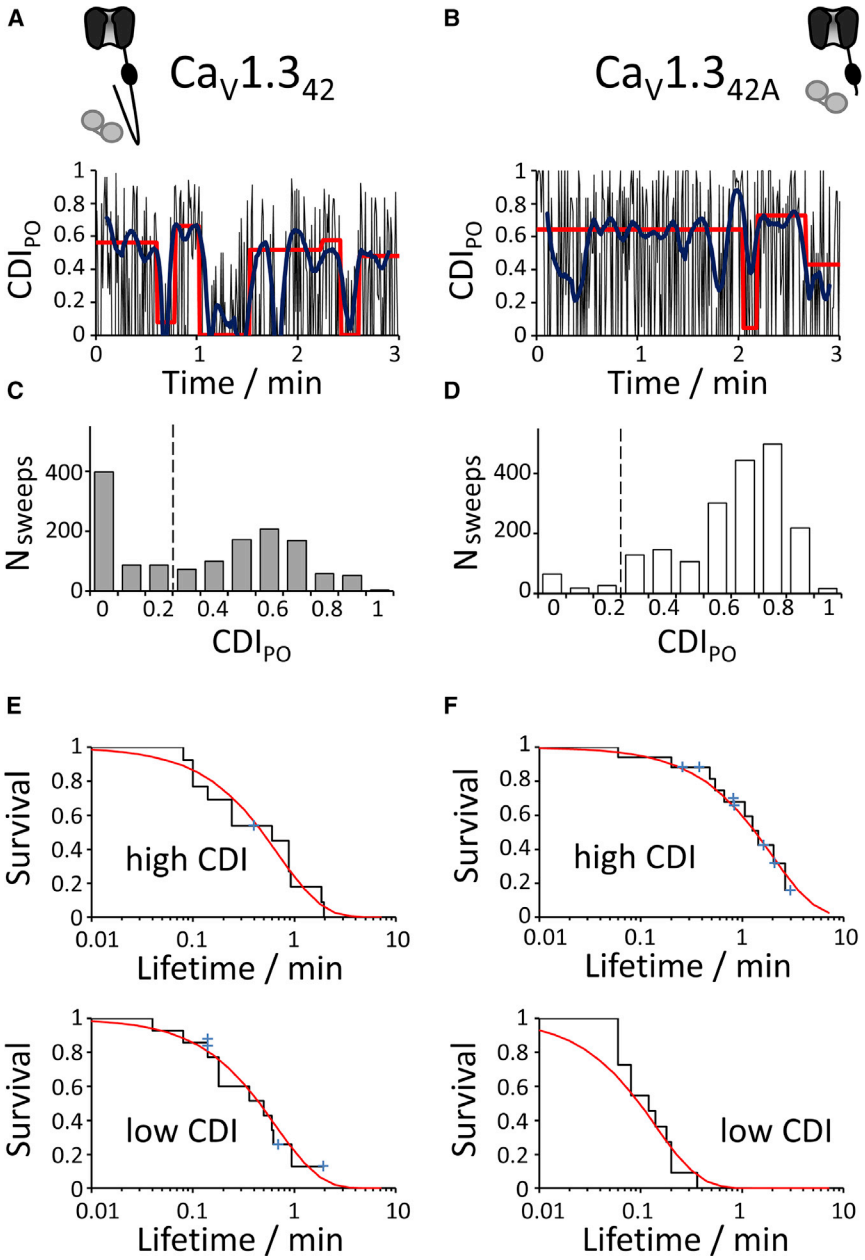

FIGURE 5 Analysis of the lifetimes of high- and low-CDI states at 0 mV. (*A* and *B*) Exemplary single-channel CDI_{PO} diaries for $Ca_V1.3_{42}$ (*A*) and $Ca_V1.3_{42A}$ (*B*) are shown. CDI_{PO} was defined as $1-P_{O\ 50–150\ ms}/\max(P_{O\ 0–50\ ms}, P_{O\ 50–150\ ms})$. Black noisy lines are CDI_{PO} calculated from individual sweeps. Dark-blue smooth lines are CDI_{PO} calculated after a Gaussian filtering of P_O diaries with a cutoff frequency of 0.33 Hz. Red stepped lines show CDI_{PO} resulting from the agglomerative clustering procedure. (*C* and *D*) Pooled histograms of CDI_{PO} calculated from the Gaussian-filtered data were used to define a threshold separating high and low CDI_{PO} peaks of $Ca_V1.3_{42}$ (*C*) and $Ca_V1.3_{42A}$ (*D*) channels. N_{sweeps} denotes the number of sweeps. (*E* and *F*) Survival curves of the low- and high-CDI states for $Ca_V1.3_{42}$ (*E*) and $Ca_V1.3_{42A}$ (*F*) fit well to a one exponential function. Black stepped lines are Kaplan-Meier estimations from the pooled data. Red smooth lines are exponential curves with decay constants equal to the calculated lifetimes of the high- and low-CDI states (Table 2).

difference in the channel activity and CDI of the channel isoforms are governed by the altered affinity of CaM to the proximal C-terminus (27). They also performed single-channel experiments with Ba^{2+} as a charge carrier and observed that apoCaM increases the channel open probability in a quantized manner. Whereas $Ca_V1.3_{42A}$ and $Ca_V1.3_{42}$ showed single distributions of the channel open probability at high and, respectively, low values, overexpression of CaM with $Ca_V1.3_{42}$ or using $Ca_V1.3_{42A}$ with an edited CaM-binding site led to the presence of two discrete peaks in P_O histograms, suggesting the binding and unbinding events of CaM.

In this work, we applied a different voltage clamp protocol to allow for a time resolution of 600 ms in single-channel P_O diaries compared to 12 s in the study mentioned above. By this, we were not only able to confirm the discrete nature of P_O regulation by CaM but also to quantify the lifetimes of putative CaM-bound (high-P_O) and CaM-absent (low-P_O) states. Furthermore, we detected sporadic CaM-binding events even in the presence of CTM ($Ca_V1.3_{42}$ isoform) at basal calcium and CaM concentrations (Ba^{2+} as a charge carrier). The overexpression of CaM together with $Ca_V1.3_{42}$ channels and the scavenging of the endogenous CaM by the coexpression of $BSCaM_{IQ}$ together with the $Ca_V1.3_{42A}$ isoform shortened and, respectively, prolonged the lifetimes of the low-P_O state in agreement with the law of mass action.

TABLE 2 Lifetimes of the High- and Low-CDI States for $Ca_V1.3$ Channels with 15 mM Ca^{2+} as a Charge Carrier at 0 mV Test Potential

	Lifetime (min)			
	$Ca_V1.3_{42}$ clusters	$Ca_V1.3_{42A}$ clusters	$Ca_V1.3_{42}$ Gaussian filter	$Ca_V1.3_{42A}$ Gaussian filter
High-CDI state	0.70×/1.4	1.8×/1.3*	0.64×/1.7	2.3×/2.4
Low-CDI state	0.66×/1.6§	0.13×/1.3*	0.44×/1.4	0.13×/2.0

Lifetimes were calculated from the pooled data. Two ways of calculations (based on the clustering or Gaussian filtering of the P_O diaries) are presented. Respective geometric mean SE factors are given after "times or divided by" symbols. The numbers of cells were 5 and 7 for $Ca_V1.3_{42}$ and $Ca_V1.3_{42A}$, respectively. Statistical significance was checked by an exact permutation test applied to the logarithm of the lifetimes. *denotes $p < 0.05$ for comparing $Ca_V1.3_{42}$ and $Ca_V1.3_{42A}$. § denotes $p < 0.05$ for comparing $Ca_V1.3_{42}$ low-CDI Ca^{2+} and low-P_O Ba^{2+} (see Table 1) lifetimes.

Our estimated lifetime of the CaM-absent state in the presence of the functional CTM of a few minutes is in remarkable agreement with the time by which a rapid increase of local CaM concentration led to an increase of the current amplitude and CDI in whole-cell experiments of Yue and co-workers (27). By contrast, for the short $Ca_V1.3$ channel isoform with attenuated CaM affinity, the induction of the current amplitude and CDI followed the time course of the increase of the local CaM (within a minute) (27).

In our single-channel experiments, $Ca_V1.3_{42}$ channels spent ~10% of the time in the high-P_O state under basal conditions. Assuming 10% of all plasmalemmal $Ca_V1.3_{42}$ channels to hold CaM (i.e., to cause an about sevenfold higher peak current then the remaining 90% of the channels and to show a CDI value of ~0.7 (27,37,50,51)), one calculates an apparent CDI of 0.3 for the whole ensemble of $Ca_V1.3_{42}$ channels. This agrees with the published values (27,33,37,38) explaining the only moderate inhibition of CDI by CTM in contrast to a nearly complete inhibition of CDI by CTM of $Ca_V1.4$ channels (32).

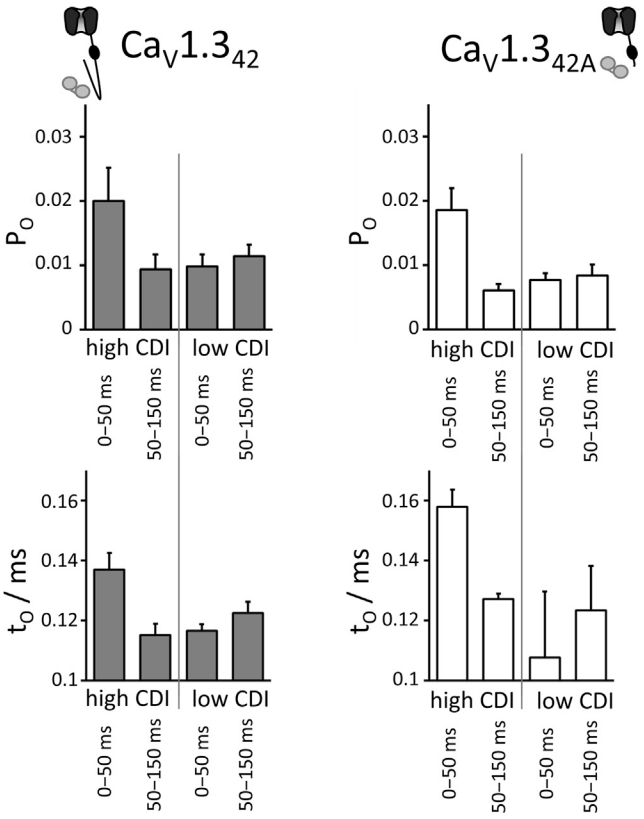

FIGURE 6 Mean open probability and mean open time (t_O) of sweeps with high- and low-CDI at 0 mV. The parameters were calculated separately for the beginning (0–50 ms) and end of the test pulse (50–150 ms). Error bars are SEM.

Our single-channel experiments with Ca^{2+} as a charge carrier also confirmed dynamic competition between CaM and CTM on a minute timescale. Visual inspection of CDI diaries at 0 mV constructed from P_O values from individual sweeps and statistical analysis of CDI diaries constructed from P_O values averaged over a few sweeps revealed that $Ca_V1.3_{42A}$ channels are predominantly in a high-CDI state, whereas $Ca_V1.3_{42}$ channels fluctuate between a high-CDI and a low-CDI state.

The presence of the time periods in which CTM is released from the proximal C-terminus because of CaM interference can permit effective interaction with other regulating proteins binding to the C-terminus. On the contrary, it is also possible that CTM provides an advantage to CaM over other proteins, which have to wait until CTM will be removed by the CaM binding. Of special interest here are CaM-like calcium-binding proteins CaBPs, which can bind concurrently with CaM and suppress CDI (41,52–55). For example, Scharinger et al. found that a disruption of the CTM function in cochlear inner hair cells led to a CDI decrease, likely because of a permitted CaBPs binding (41). Hence, CTM can allow dynamic fine-tuning of $Ca_V1.3$ channel activity for particular cellular needs.

CDI mechanism

The detailed analysis of the channel gating with Ca^{2+} as a charge carrier is in agreement with a new model of L-type Ca_V channel regulation by CaM and, thus, supports the interpretation that high-CDI states and high-P_O states correspond to the identical CaM-bound state (27,50,51). In this model, simultaneous binding of both C- and N-lobes of apoCaM to the proximal C-terminus of $Ca_V1.3$ channels is required for the switching of the channel gating from the basal low to the high-P_O mode. Upon binding of calcium to CaM, rearrangement of CaM occurs, and detachment of

one or both CaM lobes from their initial position returns the channel to its basal low-P_O activity seen as CDI. Indeed, in our experiments, initial P_O and mean open time in the high-CDI state were significantly higher than in the low-CDI state, and they dropped to the respective levels of the low-CDI state at the end of the test pulse.

Calcium and other factors, potentially influencing CaM/CTM competition

Surprisingly, $Ca_V1.3_{42}$ channels spent ~50% of the time in the high-CDI state, which was considerably more than the 10% of the high-P_O state with Ba^{2+} as a charge carrier. Respectively, the lifetime of the low-CDI state was shorter than the lifetime of the low-P_O state with Ba^{2+} as a charge carrier. It is tempting to propose that calcium can influence the efficacy of the competition between CaM and CTM of $Ca_V1.3$ channels. Moreover, at lower potentials or when using the calcium agonist (S−) Bay K 8644, the difference between isoforms was further reduced. This is in contrast to previous studies that report that the difference in current densities between Cav1.3 isoforms remained, regardless of using Ba^{2+} or Ca^{2+} as a charge carrier (33,37,50). To explain this discrepancy, we can speculate that differences in the cell culture and/or single-channel conditions may result in a different local environment of the channel.

For example, extracellular ATP can bind to endogenous purinoreceptors in HEK-293 cells activating Gi-protein and protein kinase C (56,57). Intracellular ATP influences the behavior of closely related $Ca_V1.2$ channels through a yet elusive interaction with CaM as well as an inhibition of phosphatases, thus influencing channel phosphorylation (58). In HEK-293 cells, basal phosphorylation of the C-terminus of $Ca_V1.2$ channels by protein kinase A and Ca^{2+}/CaM-dependent kinase II was shown (59,60). The phosphorylation of the sites in PCRD led to disinhibition of the channels by the distal C-terminus, presumably by interfering with PCRD/DCRD binding (59). For $Ca_V1.4$ channels, protein kinase A phosphorylation of a site in DCRD also led to a decreased affinity between distal and proximal C-terminus parts (61). Interestingly, $Ca_V1.3$ channels also have phosphorylation sites in PCRD and DCRD (62), which, depending on kinases and phosphatases status, may affect CTM binding.

Another factor, which may be influenced by experimental settings, is the concentration of available CaM (63) and probably the optional involvement of a second CaM molecule, which is either bound to the channel (64) or located in its vicinity (65). Pull-down assays (24,66–68) and fluorescence energy transfer measurements in living cells (69) show that more than one CaM molecule can bind to the proximal C-terminus of closely related $Ca_V1.2$ channels at high Ca^{2+} concentration.

Actually, Bock et al. reported that the difference between $Ca_V1.3$ isoforms can depend on Ca^{2+} concentration: CDI of $Ca_V1.3_{42A}$ and $Ca_V1.3_{43S}$, containing a proximal part of the C-terminus terminating shortly after PCRD, was similar at 15 mM Ca^{2+} but differed at 2 mM Ca^{2+} in extracellular solution (37). The fact that CTM binding to the proximal C-terminus can be antagonized by CaM in a Ca^{2+}-dependent manner as appears in our experiments was also shown for $Ca_V1.2$ channels by patch-clamp and pull-down assays (70,71). Interestingly, Crump et al. showed that, even though CTM inhibition was reversed by depolarization-induced high calcium influx, CTM still played an essential role at low potentials in decreasing quiescent cytosolic Ca^{2+} level (70).

CONCLUSION

Summing up, our single-channel experiments with Ba^{2+} and Ca^{2+} as a charge carrier demonstrate equilibrium fluctuations between the CaM-bound and the CaM-absent state of human $Ca_V1.3$ channels in the presence of the fully functional CTM. The competition between intramolecular binding of CTM and CaM association occurs on a minute timescale. Whether it can be calcium- and, thus, use-dependent at some conditions requires further investigation.

SUPPORTING MATERIAL

Supporting Materials and Methods and three figures are available at http://www.biophysj.org/biophysj/supplemental/S0006-3495(19)30061-X.

AUTHOR CONTRIBUTIONS

E.K., J.M., and S.H. designed the research and supervised the project. E.N. and W.J. performed the experiments. E.N., W.J., and E.K. analyzed the data. E.K. and S.H. wrote the manuscript with input from the all authors.

ACKNOWLEDGMENTS

We thank Sigrid Kirchmann-Hecht and Cora Fried for excellent technical assistance. We are indebted to the late David T. Yue, together with Ivy Dick and Manu Ben-Johny (Johns Hopkins University School of Medicine Baltimore, MD), for numerous insightful discussions. They, as well as Jörg Striessnig and Alexandra Koschak (University of Innsbruck, Innsbruck, Austria), provided the plasmids used in this study.

This work was supported by DFG (KU 2523/2-1 to E.K.) and Koeln Fortune Program/Faculty of Medicine, University of Cologne (2/2011 to E.K.).

REFERENCES

1. Lipscombe, D., T. D. Helton, and W. Xu. 2004. L-type calcium channels: the low down. *J. Neurophysiol.* 92:2633–2641.
2. Catterall, W. A., E. Perez-Reyes, …, J. Striessnig. 2005. International Union of Pharmacology. XLVIII. Nomenclature and structure-function relationships of voltage-gated calcium channels. *Pharmacol. Rev.* 57:411–425.
3. Zamponi, G. W., J. Striessnig, …, A. C. Dolphin. 2015. The physiology, pathology, and pharmacology of voltage-gated calcium channels and their future therapeutic potential. *Pharmacol. Rev.* 67:821–870.

4. Platzer, J., J. Engel, …, J. Striessnig. 2000. Congenital deafness and sinoatrial node dysfunction in mice lacking class D L-type Ca^{2+} channels. *Cell.* 102:89–97.
5. Matthes, J., L. Yildirim, …, S. Herzig. 2004. Disturbed atrio-ventricular conduction and normal contractile function in isolated hearts from Cav1.3-knockout mice. *Naunyn Schmiedebergs Arch. Pharmacol.* 369:554–562.
6. Zhang, Z., Y. He, …, N. Chiamvimonvat. 2005. Functional roles of Cav1.3(alpha1D) calcium channels in atria: insights gained from gene-targeted null mutant mice. *Circulation.* 112:1936–1944.
7. Baig, S. M., A. Koschak, …, H. J. Bolz. 2011. Loss of Ca(v)1.3 (CACNA1D) function in a human channelopathy with bradycardia and congenital deafness. *Nat. Neurosci.* 14:77–84.
8. McKinney, B. C., and G. G. Murphy. 2006. The L-Type voltage-gated calcium channel Cav1.3 mediates consolidation, but not extinction, of contextually conditioned fear in mice. *Learn. Mem.* 13:584–589.
9. Marschallinger, J., A. Sah, …, L. Aigner. 2015. The L-type calcium channel Cav1.3 is required for proper hippocampal neurogenesis and cognitive functions. *Cell Calcium.* 58:606–616.
10. Kim, S. H., Y. R. Park, …, C. H. Kim. 2017. Reduction of Cav1.3 channels in dorsal hippocampus impairs the development of dentate gyrus newborn neurons and hippocampal-dependent memory tasks. *PLoS One.* 12:e0181138.
11. Hurley, M. J., B. Brandon, …, D. T. Dexter. 2013. Parkinson's disease is associated with altered expression of CaV1 channels and calcium-binding proteins. *Brain.* 136:2077–2097.
12. Surmeier, D. J., J. N. Guzman, and J. Sanchez-Padilla. 2010. Calcium, cellular aging, and selective neuronal vulnerability in Parkinson's disease. *Cell Calcium.* 47:175–182.
13. Kim, S., and H. Rhim. 2011. Effects of amyloid-β peptides on voltage-gated L-type Ca(V)1.2 and Ca(V)1.3 Ca(2+) channels. *Mol. Cells.* 32:289–294.
14. Buchanan, P. J., and K. D. McCloskey. 2016. Ca_V channels and cancer: canonical functions indicate benefits of repurposed drugs as cancer therapeutics. *Eur. Biophys. J.* 45:621–633.
15. Scholl, U. I., G. Goh, …, R. P. Lifton. 2013. Somatic and germline CACNA1D calcium channel mutations in aldosterone-producing adenomas and primary aldosteronism. *Nat. Genet.* 45:1050–1054.
16. Azizan, E. A., H. Poulsen, …, M. J. Brown. 2013. Somatic mutations in ATP1A1 and CACNA1D underlie a common subtype of adrenal hypertension. *Nat. Genet.* 45:1055–1060.
17. Breitenkamp, A. F., J. Matthes, and S. Herzig. 2015. Voltage-gated calcium channels and autism spectrum disorders. *Curr. Mol. Pharmacol.* 8:123–132.
18. Pinggera, A., and J. Striessnig. 2016. Ca_v 1.3 (CACNA1D) L-type Ca^{2+} channel dysfunction in CNS disorders. *J. Physiol.* 594:5839–5849.
19. Limpitikul, W. B., I. E. Dick, …, D. T. Yue. 2016. An autism-associated mutation in CaV1.3 channels has opposing effects on voltage- and Ca(2+)-dependent regulation. *Sci. Rep.* 6:27235.
20. Pinggera, A., L. Mackenroth, …, J. Striessnig. 2017. New gain-of-function mutation shows CACNA1D as recurrently mutated gene in autism spectrum disorders and epilepsy. *Hum. Mol. Genet.* 26:2923–2932.
21. Calin-Jageman, I., and A. Lee. 2008. $Ca_{(v)}$1 L-type Ca^{2+} channel signaling complexes in neurons. *J. Neurochem.* 105:573–583.
22. Gregory, F. D., K. E. Bryan, …, A. Lee. 2011. Harmonin inhibits presynaptic Cav1.3 Ca^{2+} channels in mouse inner hair cells. *Nat. Neurosci.* 14:1109–1111.
23. Picher, M. M., A. M. Oprişoreanu, …, T. Moser. 2017. Rab interacting molecules 2 and 3 directly interact with the pore-forming $Ca_V1.3$ Ca^{2+} channel subunit and promote its membrane expression. *Front. Cell. Neurosci.* 11:160.
24. Asmara, H., E. Minobe, …, M. Kameyama. 2010. Interactions of calmodulin with the multiple binding sites of $Ca_v1.2$ Ca^{2+} channels. *J. Pharmacol. Sci.* 112:397–404.
25. Peterson, B. Z., C. D. DeMaria, …, D. T. Yue. 1999. Calmodulin is the Ca^{2+} sensor for Ca^{2+} -dependent inactivation of L-type calcium channels. *Neuron.* 22:549–558.
26. Imredy, J. P., and D. T. Yue. 1994. Mechanism of Ca(2+)-sensitive inactivation of L-type Ca^{2+} channels. *Neuron.* 12:1301–1318.
27. Adams, P. J., M. Ben-Johny, …, D. T. Yue. 2014. Apocalmodulin itself promotes ion channel opening and Ca(2+) regulation. *Cell.* 159:608–622.
28. Peterson, B. Z., J. S. Lee, …, D. T. Yue. 2000. Critical determinants of Ca(2+)-dependent inactivation within an EF-hand motif of L-type Ca(2+) channels. *Biophys. J.* 78:1906–1920.
29. Morrill, J. A., and S. C. Cannon. 2000. COOH-terminal truncated alpha(1S) subunits conduct current better than full-length dihydropyridine receptors. *J. Gen. Physiol.* 116:341–348.
30. Hulme, J. T., K. Konoki, …, W. A. Catterall. 2005. Sites of proteolytic processing and noncovalent association of the distal C-terminal domain of CaV1.1 channels in skeletal muscle. *Proc. Natl. Acad. Sci. USA.* 102:5274–5279.
31. Hulme, J. T., V. Yarov-Yarovoy, …, W. A. Catterall. 2006. Autoinhibitory control of the CaV1.2 channel by its proteolytically processed distal C-terminal domain. *J. Physiol.* 576:87–102.
32. Singh, A., D. Hamedinger, …, J. Striessnig. 2006. C-terminal modulator controls Ca^{2+}-dependent gating of Ca(v)1.4 L-type Ca^{2+} channels. *Nat. Neurosci.* 9:1108–1116.
33. Singh, A., M. Gebhart, …, A. Koschak. 2008. Modulation of voltage- and Ca^{2+}-dependent gating of $Ca_V1.3$ L-type calcium channels by alternative splicing of a C-terminal regulatory domain. *J. Biol. Chem.* 283:20733–20744.
34. Calin-Jageman, I., K. Yu, …, A. Lee. 2007. Erbin enhances voltage-dependent facilitation of Ca(v)1.3 Ca^{2+} channels through relief of an autoinhibitory domain in the Ca(v)1.3 alpha1 subunit. *J. Neurosci.* 27:1374–1385.
35. Gregory, F. D., T. Pangrsic, …, A. Lee. 2013. Harmonin enhances voltage-dependent facilitation of Cav1.3 channels and synchronous exocytosis in mouse inner hair cells. *J. Physiol.* 591:3253–3269.
36. Wahl-Schott, C., L. Baumann, …, M. Biel. 2006. Switching off calcium-dependent inactivation in L-type calcium channels by an autoinhibitory domain. *Proc. Natl. Acad. Sci. USA.* 103:15657–15662.
37. Bock, G., M. Gebhart, …, A. Koschak. 2011. Functional properties of a newly identified C-terminal splice variant of $Ca_v1.3$ L-type Ca^{2+} channels. *J. Biol. Chem.* 286:42736–42748.
38. Tan, B. Z., F. Jiang, …, T. W. Soong. 2011. Functional characterization of alternative splicing in the C terminus of L-type $Ca_V1.3$ channels. *J. Biol. Chem.* 286:42725–42735.
39. Tan, G. M., D. Yu, …, T. W. Soong. 2012. Alternative splicing at C terminus of $Ca_{(V)}$1.4 calcium channel modulates calcium-dependent inactivation, activation potential, and current density. *J. Biol. Chem.* 287:832–847.
40. Liu, X., P. S. Yang, …, D. T. Yue. 2010. Enzyme-inhibitor-like tuning of Ca(2+) channel connectivity with calmodulin. *Nature.* 463:968–972.
41. Scharinger, A., S. Eckrich, …, J. Striessnig. 2015. Cell-type-specific tuning of Cav1.3 Ca(2+)-channels by a C-terminal automodulatory domain. *Front. Cell. Neurosci.* 9:309.
42. Stanika, R., M. Campiglio, …, G. J. Obermair. 2016. Splice variants of the $Ca_V1.3$ L-type calcium channel regulate dendritic spine morphology. *Sci. Rep.* 6:34528.
43. Vincent, P. F., Y. Bouleau, …, D. Dulon. 2017. Different $Ca_V1.3$ channel isoforms control distinct components of the synaptic vesicle cycle in auditory inner hair cells. *J. Neurosci.* 37:2960–2975.
44. Black, D. J., J. Leonard, and A. Persechini. 2006. Biphasic Ca^{2+}-dependent switching in a calmodulin-IQ domain complex. *Biochemistry.* 45:6987–6995.
45. Koch, P., S. Herzig, and J. Matthes. 2016. An expert protocol for immunofluorescent detection of calcium channels in tsA-201 cells. *J. Pharmacol. Toxicol. Methods.* 82:20–25.

46. Schröder, F., and S. Herzig. 1999. Effects of β_2-adrenergic stimulation on single-channel gating of rat cardiac L-type Ca^{2+} channels. *Am. J. Physiol.* 276:H834–H843.

47. Jangsangthong, W., E. Kuzmenkina, …, S. Herzig. 2011. Single-channel monitoring of reversible L-type Ca(2+) channel Ca(V)α(1)-Ca(V)β subunit interaction. *Biophys. J.* 101:2661–2670.

48. Ben Johny, M., P. S. Yang, …, D. T. Yue. 2013. Dynamic switching of calmodulin interactions underlies Ca^{2+} regulation of CaV1.3 channels. *Nat. Commun.* 4:1717.

49. Josephson, I. R., A. Guia, …, M. D. Stern. 2010. Ca(2+)-dependent components of inactivation of unitary cardiac L-type Ca(2+) channels. *J. Physiol.* 588:213–223.

50. Liu, N., Y. Yang, …, X. Liu. 2017. Cooperative and acute inhibition by multiple C-terminal motifs of L-type Ca^{2+} channels. *eLife.* 6:e21989.

51. Banerjee, R., J. B. Yoder, …, M. Ben-Johny. 2018. Bilobal architecture is a requirement for calmodulin signaling to $Ca_V1.3$ channels. *Proc. Natl. Acad. Sci. USA.* 115:E3026–E3035.

52. Cui, G., A. C. Meyer, …, A. Lee. 2007. Ca^{2+}-binding proteins tune Ca^{2+}-feedback to Cav1.3 channels in mouse auditory hair cells. *J. Physiol.* 585:791–803.

53. Yang, P. S., B. A. Alseikhan, …, D. T. Yue. 2006. Switching of Ca^{2+}-dependent inactivation of Ca(v)1.3 channels by calcium binding proteins of auditory hair cells. *J. Neurosci.* 26:10677–10689.

54. Yang, P. S., M. B. Johny, and D. T. Yue. 2014. Allostery in Ca^{2+} channel modulation by calcium-binding proteins. *Nat. Chem. Biol.* 10:231–238.

55. Hardie, J., and A. Lee. 2016. Decalmodulation of Cav1 channels by CaBPs. *Channels (Austin).* 10:33–37.

56. Wirkner, K., J. Schweigel, …, P. Illes. 2004. Adenine nucleotides inhibit recombinant N-type calcium channels *via* G protein-coupled mechanisms in HEK 293 cells; involvement of the $P2Y_{13}$ receptor-type. *Br. J. Pharmacol.* 141:141–151.

57. Scholze, A., T. D. Plant, …, B. Nürnberg. 2001. Functional expression and characterization of a voltage-gated CaV1.3 (alpha1D) calcium channel subunit from an insulin-secreting cell line. *Mol. Endocrinol.* 15:1211–1221.

58. Minobe, E., M. X. Mori, and M. Kameyama. 2017. Calmodulin and ATP support activity of the Cav1.2 channel through dynamic interactions with the channel. *J. Physiol.* 595:2465–2477.

59. Fuller, M. D., M. A. Emrick, …, W. A. Catterall. 2010. Molecular mechanism of calcium channel regulation in the fight-or-flight response. *Sci. Signal.* 3:ra70.

60. Minobe, E., S. Maeda, …, M. Kameyama. 2014. A new phosphorylation site in cardiac L-type Ca^{2+} channels (Cav1.2) responsible for its cAMP-mediated modulation. *Am. J. Physiol. Cell Physiol.* 307:C999–C1009.

61. Sang, L., I. E. Dick, and D. T. Yue. 2016. Protein kinase A modulation of CaV1.4 calcium channels. *Nat. Commun.* 7:12239.

62. Ramadan, O., Y. Qu, …, M. Boutjdir. 2009. Phosphorylation of the consensus sites of protein kinase A on α_{1D} L-type calcium channel. *J. Biol. Chem.* 284:5042–5049.

63. Black, D. J., Q. K. Tran, and A. Persechini. 2004. Monitoring the total available calmodulin concentration in intact cells over the physiological range in free Ca^{2+}. *Cell Calcium.* 35:415–425.

64. Kim, E. Y., C. H. Rumpf, …, D. L. J. Minor, Jr. 2010. Multiple C-terminal tail Ca(2+)/CaMs regulate Ca(V)1.2 function but do not mediate channel dimerization. *EMBO J.* 29:3924–3938.

65. Saucerman, J. J., and D. M. Bers. 2012. Calmodulin binding proteins provide domains of local Ca^{2+} signaling in cardiac myocytes. *J. Mol. Cell. Cardiol.* 52:312–316.

66. Shao, D., M. Zhao, …, L. Hao. 2014. The individual N- and C-lobes of calmodulin tether to the Cav1.2 channel and rescue the channel activity from run-down in ventricular myocytes of guinea-pig heart. *FEBS Lett.* 588:3855–3861.

67. He, G., F. Guo, …, L. Hao. 2013. Lobe-related concentration- and Ca(2+)-dependent interactions of calmodulin with C- and N-terminal tails of the CaV1.2 channel. *J. Physiol. Sci.* 63:345–353.

68. Minobe, E., H. Asmara, …, M. Kameyama. 2011. Calpastatin domain L is a partial agonist of the calmodulin-binding site for channel activation in Cav1.2 Ca^{2+} channels. *J. Biol. Chem.* 286:39013–39022.

69. Ben-Johny, M., D. N. Yue, and D. T. Yue. 2016. Detecting stoichiometry of macromolecular complexes in live cells using FRET. *Nat. Commun.* 7:13709.

70. Crump, S. M., D. A. Andres, …, J. Satin. 2013. The cardiac L-type calcium channel distal carboxy terminus autoinhibition is regulated by calcium. *Am. J. Physiol. Heart Circ. Physiol.* 304:H455–H464.

71. Lyu, L., Q. Gao, …, M. Kameyama. 2017. A new interaction between proximal and distal C-terminus of Cav1.2 channels. *J. Pharmacol. Sci.* 133:240–246.